Potential-energy surface for the electronic ground state of NH_3 up to $20\,000\ cm^{-1}$ above equilibrium

Sergei N. Yurchenko, Jingjing Zheng, Hai Lin, Per Jensen, and Walter Thiel

Citation: J. Chem. Phys. **123**, 134308 (2005); doi: 10.1063/1.2047572
View online: https://doi.org/10.1063/1.2047572
View Table of Contents: http://aip.scitation.org/toc/jcp/123/13
Published by the American Institute of Physics

Potential-energy surface for the electronic ground state of NH_3 up to 20 000 cm^{-1} above equilibrium

Sergei N. Yurchenko and Jingjing Zheng
Max-Planck-Institut für Kohlenforschung, Kaiser-Wilhelm-Platz 1, D-45470 Mülheim an der Ruhr, Germany

Hai Lin
Chemistry Department, University of Colorado at Denver and Health Science Center, Campus Box 194, P.O. Box 173364, Denver, Colorado 80217

Per Jensen
Fachbereich C-Theoretische Chemie, Bergische Universität, D-42097 Wuppertal, Germany

Walter Thiel[a)]
Max-Planck-Institut für Kohlenforschung, Kaiser-Wilhelm-Platz 1, D-45470 Mülheim an der Ruhr, Germany

(Received 27 July 2005; accepted 9 August 2005; published online 3 October 2005)

Ab initio coupled cluster calculations with single and double substitutions and a perturbative treatment of connected triple excitations [CCSD(T)] with the augmented correlation-consistent polarized valence triple-zeta aug-cc-pVTZ basis at 51 816 geometries provide a six-dimensional potential-energy surface for the electronic ground state of NH_3. At 3814 selected geometries, CBS+ energies are obtained by extrapolating the CCSD(T) results for the aug-cc-pV*XZ*(X=T,Q,5) basis sets to the complete basis set (CBS) limit and adding corrections for core-valence correlation and relativistic effects. CBS** *ab initio* energies are generated at 51 816 geometries by an empirical extrapolation of the CCSD(T)/aug-cc-pVTZ results to the CBS+ limit. They cover the energy region up to 20 000 cm^{-1} above equilibrium. Parametrized analytical functions are fitted through the *ab initio* points. For these analytical surfaces, vibrational term values and transition moments are calculated by means of a variational program employing a kinetic-energy operator expressed in the Eckart-Sayvetz frame. Comparisons against experiment are used to assess the quality of the generated potential-energy surfaces. A "spectroscopic" potential-energy surface of NH_3 is determined by a slight empirical adjustment of the *ab initio* potential to the experimental vibrational term values. Variational calculations on this refined surface yield rms deviations from experiment of 0.8 cm^{-1} for 24 inversion splittings and 0.4 (3.0) cm^{-1} for 34 (51) vibrational term values up to 6100 (10 300) cm^{-1}. © *2005 American Institute of Physics*. [DOI: 10.1063/1.2047572]

I. INTRODUCTION

We report an extension of our previous *ab initio* study[1] on the potential-energy surface (PES) of the electronic ground state of NH_3 at the CCSD(T) level. The basic approach is the same as before:[1] CCSD(T) energies obtained with the aug-cc-pV*XZ* basis sets (X=T,Q,5) in the frozen-core approximation are empirically extrapolated to the complete basis-set (CBS) level. CBS+ energies are determined by correcting the CBS energies for core-valence correlation and relativistic effects. The differences between the CCSD(T)/CBS+ and CCSD(T)/aug-cc-pVTZ energies that are available at a limited set of geometries are used to derive an analytical representation of the corresponding energy difference surface (EDS), which is then employed to correct the CCSD(T)/aug-cc-pVTZ energies at all nuclear geometries and thereby generate so-called CBS** energies. Proceeding in this manner, we have now constructed potential surfaces that completely cover the energy region up to 20 000 cm^{-1} above equilibrium, which is a substantial extension of our previous work.[1] In addition to the surfaces presented here, other high-level potential-energy surfaces have recently been computed for the electronic ground state of NH_3.[2–6] The most recent of these studies has gone beyond the CCSD(T) level and incorporated higher excitations in the coupled cluster series up to CCSDTQP and an extrapolation to the full configuration-interaction (CI) limit as well as diagonal Born-Oppenheimer corrections.[6]

The computed *ab initio* energies are used to determine parametrized analytical representations of the potential-energy surface, based on an expansion in terms of geometrically defined coordinates.[1] These analytical potential-energy functions and analogous parametrizations of the dipole moment surfaces[7,8] serve as input for variational calculations performed in the framework of a recently developed model for the nuclear motion in pyramidal XY_3 molecules.[1,9] It has already been demonstrated that such calculations can provide accurate rotation-vibration energies[9] and rotation-vibration spectra[7,8] of $^{14}NH_3$.

The analytical representation of the potential-energy surface should ideally satisfy the following criteria:[10,11] It should be global (i.e., with correct behavior not only near

a)Author to whom correspondence should be addressed. Electronic mail: thiel@mpi-muelheim.mpg.de

equilibrium, but also in the asymptotic limits), flexible (i.e., capable of accommodating a large number of parameters), but compact (using rather few parameters in practice), and robust (in that small variations of parameters lead only to small variations of the potential-energy surface). Our expansion in terms of geometrically defined coordinates is flexible since it can be taken to arbitrarily high order, and it has an at least qualitatively correct asymptotic behavior.[10] In the present work, the *ab initio* data sets are significantly larger than those considered before,[1] so that it is inevitable to introduce more parameters in the analytical representation. This sacrifices to some extent its compactness and robustness, but is the price to be paid for obtaining a potential-energy surface that is valid in a larger region of coordinate space.

We present several analytical representations of the potential-energy surface for the electronic ground state of NH_3 which differ by the level of theory in the underlying *ab initio* calculations, and by the amount of *ab initio* data used during the fits. Their quality is assessed by considering the properties of the fits through the *ab initio* points [root mean square (rms) deviation and number of parameters varied] and by comparing calculated vibrational term values and transition moments with the available experimental information. The comparison between theory and experiment for vibrational term values is a traditional test for potential-energy surfaces of NH_3,[1–5,9,12–21] and corresponding comparisons for vibrational transition moments are customarily used to gauge the quality of computed dipole moment surfaces of NH_3.[7,8,22–24]

The comparisons against experiment indicate that our present *ab initio* surfaces are quite accurate, but not perfect. Further improvements in a purely *ab initio* fashion would require calculations at higher levels, for example by incorporating higher excitations in the coupled cluster series.[6,25] We have chosen to explore the alternative empirical approach of refining the *ab initio* potential-energy surface against experimental data. The corresponding fit has been restrained to remain close to our best purely *ab initio* surface.

The paper is structured as follows. Section II describes the *ab initio* methods employed and defines the selected sets of nuclear geometries. Section III specifies the procedure for determining the CBS** energies. The analytical representation of the potential-energy function is the subject of Sec. IV, and Sec. V gives the details of the variational nuclear-motion calculations. Section VI discusses the properties of the analytical potential-energy surfaces and compares the variational results for the *ab initio* surfaces against experiment. Section VII presents a refined PES obtained from a restrained fit to experimental data. Finally, Sec. VIII offers a discussion and conclusions.

II. DEFINITION OF THE *AB INITIO* DATA SETS

A. Computational scheme

The quantum-chemical calculations were done at the CCSD(T) level (coupled cluster theory with all single and double substitutions from the Hartree-Fock reference determinant[26] augmented by a perturbative treatment of connected triple excitations[27,28]) using the MOLPRO2000 package.[29,30] The correlation-consistent families of basis sets cc-pV*X*Z, aug-cc-pV*X*Z, and aug-cc-pCV*X*Z(X=T,Q,5) developed by Dunning[31] and Woon and Dunning[32] were employed. CCSD(T) calculations with the cc-pV*X*Z, aug-cc-pV*X*Z, and aug-cc-pCV*X*Z basis sets are denoted by *X*Z, A*X*Z, and AC*X*Z, respectively. An appended label "fc" ("cc") indicates that the frozen-core approximation was (was not) applied. Threshold values for MOLPRO2000 were the same as before.[1]

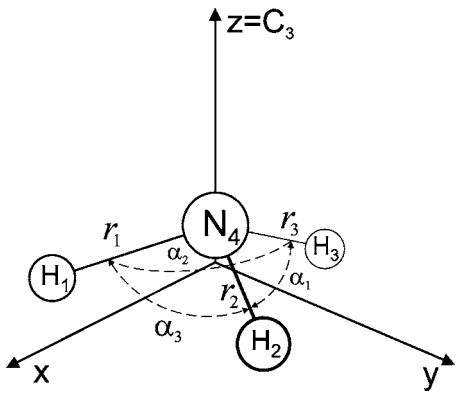

FIG. 1. The labeling of the nuclei, the molecule-fixed axis system *xyz*, and the geometrically defined coordinates chosen for NH_3.

ATZfc calculations were performed at all geometries considered. CBS extrapolation at selected geometries requires ATZfc, AQZfc, and A5Zfc energies. Denoting the cardinal quantum number of the basis set by X, with X=3 for ATZfc, 4 for AQZfc, and 5 for A5Zfc, the computed energies were fitted by the expression[33,34]

$$E(X) = E_\infty + b/X^3 \tag{1}$$

to determine the CBS energy E_∞ at the complete basis-set limit and a second fit parameter b.

The CBS energy was corrected for core-valence correlation and relativistic effects. The core-valence correlation contribution ΔE_{core} was obtained as the energy difference between frozen-core (ACTZfc) and all-electron (ACTZcc) calculations. The relativistic correction ΔE_{rel} was evaluated at the ATZfc level as the sum of the expectation values for the mass-velocity and the one-electron Darwin terms. The final corrected energy is given by $E_{\text{corr}}=E_\infty+\Delta E_{\text{core}}+\Delta E_{\text{rel}}$ and called the CBS+ energy.

Dipole moment surfaces were computed at the ATZfc level using a numerical finite-difference procedure with an added dipole field of 0.005 a.u.

B. Data sets

The bond length r_i is the instantaneous value of the distance N–H_i, where H_i is the proton labeled i=1, 2, or 3 in NH_3. The bond angles α_i are denoted as $\alpha_1=\angle(H_2NH_3)$, $\alpha_2=\angle(H_1NH_3)$, and $\alpha_3=\angle(H_1NH_2)$ (see Fig. 1). In terms of these coordinates, we define three six-dimensional grids: 6D-1, a dense grid where $r_i/\text{Å} \in \{0.85, 0.90, 0.95, 0.99, 1.01, 1.05, 1.10, 1.20\}$ and $\alpha_i \in \{80°, 90°, 110°, 104°, 108°, 112°, 116°, 120°\}$ (14 400 grid points); 6D-2, a grid with points close to equilibrium, $r_i/\text{Å} \in \{0.99, 1.01, 1.05\}$ and α_i

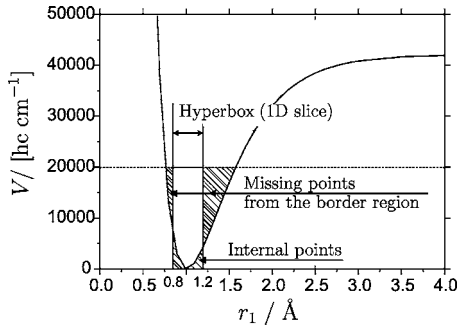

FIG. 2. Potential curve along the stretching coordinate r_1 at the ATZfc level of theory. The remaining five coordinates are fixed at $r_2=r_3=1.012$ Å, $\alpha_1=\alpha_2=\alpha_3=106.7°$. The 6D-4 grid points (see text) and the symmetrically equivalent points form a "hyperbox" in coordinate space that contains the internal points.

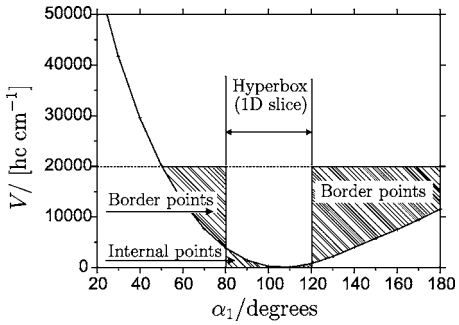

FIG. 3. Potential curve along the bending coordinate a_1 at the ATZfc level of theory. The remaining five coordinates are fixed at $r_1=r_2=r_3=1.012$ Å, $\alpha_2=\alpha_3=106.7°$. For further conventions see Fig. 2.

$\in\{98°, 104°, 108°, 112°, 116°\}$ (560 grid points); and 6D-3, a sparse grid where $r_i/\text{Å}\in\{0.85, 0.99, 1.05, 1.20\}$ and $\alpha_i\in\{80°, 90°, 101°, 112°, 120°\}$ (700 grid points). These grids were used in our previous *ab initio* study.[1] For a given grid, a complete set of points could in principle be generated by forming all combinations of $(r_1, r_2, r_3, \alpha_1, \alpha_2, \alpha_3)$ that are consistent with the "allowed" values of r_i and α_i. For the 6D-1 grid, for example, there are eight allowed values for each coordinate, and the total number of possible grid points is thus $8^6=262\,144$. However, the potential energy of NH_3 is invariant to permutations of the three protons,[35,36] and many of these 262 144 grid points are connected by nuclear permutations and hence correspond to the same electronic energy. For the three grids, 6D-1, 6D-2, and 6D-3, we previously[1] reduced the number of points further (to reduce the computational effort) by imposing the constraints $r_1\leqslant r_2\leqslant r_3$ and $\alpha_1\leqslant\alpha_2\leqslant\alpha_3$. This leads to the 14 400, 560, and 700 points listed above for the 6D-1, 6D-2, and 6D-3 grids, respectively. If one applies only the constraint $r_1\leqslant r_2\leqslant r_3$ and then removes all symmetrically redundant points from the remaining geometries, the 6D-1, 6D-2, and 6D-3 grids contain 45 760, 680, and 1540 points, respectively. In the present work we use the 45 760-point grid obtained in this manner from the 6D-1 allowed values of r_i and α_i. The resulting grid is called 6D-4 and has the range of $0.85\ \text{Å}\leqslant r_1\leqslant r_2\leqslant r_3\leqslant 1.20$ Å and $80°\leqslant\alpha_1,\alpha_2,\alpha_3\leqslant 120°$. The energies calculated at the 6D-4 grid points extend up to 36 800 cm^{-1} above equilibrium.

Since we aim at a consistent description of the electronic ground-state potential-energy surface of NH_3 for energies up to 20 000 cm^{-1} above equilibrium, we need to check for low-energy points outside the 6D-"hyperbox" containing the 6D-4 grid points and symmetrically equivalent points. The one-dimensional potential curves in Figs. 2 and 3 show that such low-energy points exist. We thus have to find a "border" in the six-dimensional coordinate space that envelopes the geometries with a potential energy of up to 20 000 cm^{-1} which we need to cover with *ab initio* points. Exploratory calculations with our previous analytical representation of the ATZfc potential-energy surface[1] suggested that it is sufficient to consider geometries with $0.75\ \text{Å}\leqslant r_i\leqslant 1.60$ Å and $45°\leqslant\alpha_i\leqslant 180°$ for this purpose. *Ab initio* calculations at the ATZfc level further narrowed the range of relevant geometries and led to the definition of a "border search grid" 6D-B with the allowed values $r_i/\text{Å}\in\{0.90, 1.00, 1.10, 1.25, 1.40, 1.55\}$ and $\alpha_i\in\{45.0°, 60.0°, 75.0°, 90.0°, 105.0°, 120.0°, 135.0°, 150.0°, 165.0°, 180.0°\}$. The range of allowed values was chosen such that the energy remains in the target region when one internal coordinate is displaced while keeping the others close to their optimum values. Simultaneous displacements along two or more internal coordinates will generally yield (much) higher energies, and it is clearly unnecessary to perform *ab initio* calculations at such severely distorted geometries that will formally be part of the 6D-B grid. Such geometries were identified through an initial screening with the analytical potential-energy function. Proceeding in this manner, 6056 points with energies below 20 000 cm^{-1} were found by ATZfc *ab initio* calculations on the 6D-B grid (not counting the corresponding symmetrically equivalent points).

The union of the 45 760 points of the 6D-4 grid with the 6056 points of the 6D-B grid generates the extended grid 6D-5 with 51 816 points. At the ATZfc level, 29 860 of these points have energies below 10 000 cm^{-1}, 20 213 points lie between 10 000 and 20 000 cm^{-1}, and the remaining 1743 points have energies above 20 000 cm^{-1}. Since the 6D-4 grid is contained in the 6D-5 grid, the ATZfc energies range up to 36 800 cm^{-1} above equilibrium in both cases, but the coverage is designed to be adequate only up to 20 000 cm^{-1}.

The CBS+ calculations are more demanding than the ATZfc calculations (see Sec. II A). Therefore only 2554 CBS+ energies were computed in the border region, for a subset of the ATZfc points on the 6D-B grid. These 2554 points were combined with the 1260 internal points of the 6D-2 and 6D-3 grids (where CBS+ energies were determined previously[1]) to yield the 6D-6 grid.

Table I summarizes the available *ab initio* data sets. ATZfc energies have been computed previously[1] for the 6D-1 grid. The present work provides ATZfc energies for the 6D-4 and 6D-5 grids as well as CBS+ energies for the 6D-6 grid, which can be used to determine the CBS**-energies for the 6D-4 and 6D-5 grids (see Sec. III). For easy reference, Table I also contains the labels of the analytical potential functions that represent the *ab initio* data sets (see Sec. IV).

The T1 diagnostic test[37] was applied to all 51 816 ATZfc points to ensure that the CCSD(T) treatment is adequate for all geometries considered. The largest T1 value obtained was 0.019.

TABLE I. Notation for the grids, the *ab initio* data sets, and the analytical representations of the potential-energy surfaces employed for NH_3.

Grid	Data set[a]	PES[b]
6D-1	ATZfc-14 400	ATZfc-1
6D-4	ATZfc-45 760	ATZfc-4
6D-5	ATZfc-51 816	ATZfc-5
6D-6	CBS+-3 814	CBS+
6D-4	CBS**-45 760	CBS**-4
6D-5	CBS**-51 816	CBS**-5

[a]The number in the data set label is the number of *ab initio* points in the underlying grid.
[b]Analytical representation of the potential-energy surface (see Sec. IV).

III. CBS** SURFACES

In this section we discuss a procedure that aims at improving the ATZfc data by utilizing the available, more accurate CBS+ energies. The basic approach is to calculate the differences $\Delta E = E(\mathrm{CBS+}) - E(\mathrm{ATZfc})$ at all geometries where $E(\mathrm{CBS+})$ is available, to represent these differences by an empirical correction function that depends on the nuclear coordinates, and then to add the value of this correction function to $E(\mathrm{ATZfc})$ at all available geometries. The resulting energies are expected to approach CBS+ quality at all geometries where $E(\mathrm{ATZfc})$ is known.

Previously, the correction was done in terms of Cartesian coordinates and cubic spline interpolation[1] which led to CBS* energies. The disadvantage of spline interpolation is that it requires a regular grid for numerical differentiation. Alternatively, the correction function can be expressed as a polynomial in terms of the geometrically defined coordinates r_i and α_i, with the coefficients being obtained by least-squares fitting. We adopt this latter approach here to generate CBS** energies simply because the "border points" are not defined on a regular grid. It should be noted, however, that the CBS** energies from fitting are usually less reliable than the CBS* energies from interpolation, especially at highly distorted geometries.[1]

To be more specific, the CBS**-51 816 surface was constructed by calculating $\Delta E = E(\mathrm{CBS+}) - E(\mathrm{ATZfc})$ at all 3814 points of the 6D-6 grid, fitting a sextic polynomial in r_i and α_i through the resulting ΔE values, and adding the value of the fitted polynomial to $E(\mathrm{ATZfc})$ at all 51 816 points of the 6D-5 grid. The rms deviation between the CBS+ and CBS** surfaces at the 3814 geometries of the 6D-6 grid is 2.8 cm^{-1}. Thus, the computed CBS+ energies are well reproduced by the CBS** surface.

A sextic polynomial was chosen to represent the correction function because it produces the best fit to the ΔE values. As the order of the chosen polynomial is increased, the rms deviations of the fit to the ΔE values decrease in a satisfactory manner, from 7.4 cm^{-1} (cubic) via 5.7 cm^{-1} (quartic) and 4.0 cm^{-1} (quintic) to 2.8 cm^{-1} (sextic). A seventh-order polynomial did not give useful results because the number of fit parameters required was comparable to the number of *ab initio* points available so that the fit diverged. The sextic polynomial seems to represent the correction function rather uniformly at all geometries. For example, the rms deviation drops only slightly from 2.8 to 2.6 cm^{-1} when all border points are removed from the 6D-5 grid. The consistency of the chosen approach can also be appreciated from the difference between the two CBS**-51 816 surfaces generated by quintic and sextic correction functions, respectively: the corresponding rms deviation is 3.5 cm^{-1}.

In addition to the full CBS**-51 816 data set (6D-5 grid), a reduced CBS**-45 760 data set (6D-4 grid) has been constructed in a completely analogous manner. The 6D-4 grid does not contain the border points with their distorted geometries.

IV. ANALYTICAL REPRESENTATION OF THE POTENTIAL-ENERGY FUNCTION

For each of the *ab initio* data sets in Table I, an analytical representation has been determined by fitting a function of the following form[1] through the *ab initio* points:

$$\begin{aligned} V(\xi_1,\xi_2,\xi_3,\xi_{4a},\xi_{4b};\sin\bar{\rho}) &= V_e + V_0(\sin\bar{\rho}) + \sum_j F_j(\sin\bar{\rho})\xi_j + \sum_{j\leqslant k} F_{jk}(\sin\bar{\rho})\xi_j\xi_k \\ &+ \sum_{j\leqslant k\leqslant l} F_{jkl}(\sin\bar{\rho})\xi_j\xi_k\xi_l + \sum_{j\leqslant k\leqslant l\leqslant m} F_{jklm}(\sin\bar{\rho})\xi_j\xi_k\xi_l\xi_m \\ &+ \sum_{j\leqslant k\leqslant l\leqslant m\leqslant n} F_{jklmn}(\sin\bar{\rho})\xi_j\xi_k\xi_l\xi_m\xi_n \\ &+ \sum_{j\leqslant k\leqslant l\leqslant m\leqslant n\leqslant o} F_{jklmno}(\sin\bar{\rho})\xi_j\xi_k\xi_l\xi_m\xi_n\xi_o. \end{aligned} \tag{2}$$

The variables are

$$\xi_k = 1 - \exp(-a(r_k - r_e)), \quad k = 1,2,3, \tag{3}$$

$$\xi_{4a} = \frac{1}{\sqrt{6}}(2\alpha_1 - \alpha_2 - \alpha_3), \tag{4}$$

$$\xi_{4b} = \frac{1}{\sqrt{2}}(\alpha_2 - \alpha_3), \tag{5}$$

where r_e denotes the equilibrium value of r_k, and

$$\sin\bar{\rho} = \frac{2}{\sqrt{3}}\sin[(\alpha_1 + \alpha_2 + \alpha_3)/6]. \tag{6}$$

The pure inversion potential-energy function in Eq. (2) is taken to be

$$V_0(\sin\bar{\rho}) = \sum_{s=1}^{8} f_0^{(s)}(\sin\rho_e - \sin\bar{\rho})^s, \tag{7}$$

and the functions $F_{jk\ldots}(\sin\bar{\rho})$ are defined as

$$F_{jk\ldots}(\sin\bar{\rho}) = \sum_{s=0}^{N} f_{jk\ldots}^{(s)}(\sin\rho_e - \sin\bar{\rho})^s, \tag{8}$$

where $\sin\rho_e$ is the equilibrium value of $\sin\bar{\rho}$, a is a molecular parameter, and the quantities $f_0^{(s)}$ and $f_{jk\ldots}^{(s)}$ in Eqs. (7) and (8) are expansion coefficients. The summation limits in Eq. (8) are $N=6$ for $F_j(\sin\bar{\rho})$, $N=4$ for $F_{jk}(\sin\bar{\rho})$, $N=3$ for $F_{jkl}(\sin\bar{\rho})$, $N=2$ for $F_{jklm}(\sin\bar{\rho})$, $F_{jklmn}(\sin\bar{\rho})$, and $F_{jklmno}(\sin\bar{\rho})$. In total there are 303 symmetrically unique

TABLE II. CBS**-5 potential-energy parameters (in cm^{-1} unless otherwise indicated) up to fourth order for the electronic ground state of NH_3, see Eq. (2). Conventions for indices: 4=4*a* and 5=4*b*. Only symmetrically unique parameters are given. Symmetry relations between the parameters are available as supplementary material (see Ref. 38) together with a FORTRAN routine for calculating potential-energy values. The quantities in parentheses are standard errors in units of the last digit.

Parameter	Value	Parameter	Value	Parameter	Value
ρ_e/deg	112.096 6(16)	f_{44}^3	324 179(1399)	f_{1111}^0	3 694.9(85)
r_e/Å	1.010 313 1(59)	f_{44}^4	−536 600(6670)	f_{1111}^1	−6 990(133)
$a/Å^{-1}$	2.15	f_{111}^0	277.2(14)	f_{1111}^2	19 038(542)
V_e	−12 419 377.33(78)	f_{111}^1	−9 581(23)	f_{1112}^0	−545.7(25)
f_0^2	324 077(35)	f_{111}^2	61 987(367)	f_{1112}^2	14 424(756)
f_0^3	−401 792(343)	f_{111}^3	−262 799(2146)	f_{1114}^0	−678.5(98)
f_0^4	1 133 218(4844)	f_{112}^0	−291.8(13)	f_{1114}^2	−59 594(777)
f_0^5	−2 662 929(36894)	f_{112}^1	2 294(15)	f_{1122}^0	−189.9(34)
f_0^6	4 561 862(83100)	f_{112}^2	26 099(312)	f_{1122}^2	14 272(605)
f_1^1	−33 671.7(42)	f_{112}^3	−103 127(1765)	f_{1123}^0	−254.3(31)
f_1^2	41 558(72)	f_{114}^0	−2 068.4(25)	f_{1123}^1	2 729(51)
f_1^3	−349 715(693)	f_{114}^1	−6 903(36)	f_{1124}^0	895.1(45)
f_1^4	1 246 471(6848)	f_{114}^2	−77 502(428)	f_{1124}^1	2 070(92)
f_1^5	−2 439 730(21652)	f_{114}^3	233 336(2638)	f_{1124}^2	−7 392(723)
f_{11}^0	38 730.1(10)	f_{123}^0	−186.3(57)	f_{1125}^0	1 399.4(52)
f_{11}^1	−17 346(15)	f_{123}^1	4 547(43)	f_{1125}^1	5 090(56)
f_{11}^2	57 866(175)	f_{123}^2	16 600(869)	f_{1144}^0	−1 150.3(74)
f_{11}^3	−462 520(1598)	f_{123}^3	−88 441(5419)	f_{1144}^1	−7 205(77)
f_{11}^4	979 992(7042)	f_{124}^0	1 956.59(96)	f_{1155}^0	−2 615.7(81)
f_{12}^0	−403.29(72)	f_{124}^1	5 405(28)	f_{1155}^1	−8 539(151)
f_{12}^1	4 673(12)	f_{124}^2	−2 685(197)	f_{1244}^0	508.2(43)
f_{12}^2	41 577(182)	f_{144}^0	−1 648.6(21)	f_{1244}^2	−27 657(596)
f_{12}^3	−199 083(1988)	f_{144}^1	−6 830(36)	f_{1255}^0	1 321.9(45)
f_{12}^4	606 382(8584)	f_{144}^2	−19 840(613)	f_{1255}^1	921(61)
f_{14}^0	−3 651(11)	f_{144}^3	85 887(2549)	f_{1444}^0	−765.1(53)
f_{14}^1	−17 081(16)	f_{155}^0	−2 938.1(22)	f_{1444}^1	−3 922(69)
f_{14}^2	−44 594(211)	f_{155}^1	−9 414(45)	f_{1455}^0	−1 581.9(91)
f_{14}^3	156 439(2117)	f_{155}^2	−14 906(611)	f_{1455}^1	−8 474(169)
f_{14}^4	−427 396(8779)	f_{155}^3	−119 102(2480)	f_{1455}^2	−93 060(1380)
f_{44}^0	16 833.16(77)	f_{455}^0	1 551.7(33)	f_{4444}^0	395.6(12)
f_{44}^1	67 883(18)	f_{455}^1	−57 777(49)	f_{4444}^1	8 421(53)
f_{44}^2	−110 704(213)	f_{455}^2	35 451(946)	f_{4444}^2	13 895(551)
f_{44}^3	324 179(1399)	f_{455}^3	388 038(3465)		

potential parameters $f_{jk\ldots}^{(s)}$. The symmetry relations between the parameters are given as supplementary material.[38]

Considering the large *ab initio* data sets with more than 45 000 points, it is unavoidable to vary a large number of potential parameters in the fits, even though we use a reasonable analytical representation of the potential-energy surface. For a satisfactory description of the border points with their often highly distorted geometries, the expansion in Eq. (2) must be taken to sixth order whereas a fourth-order expansion was sufficient in the previous fits that involved only regular points.[1] To give a specific example, the present sixth-order fit of the ATZfc-51 816 data set (6D-5) with 171 varied parameters achieves a rms deviation of 3.5 cm^{-1}, while the previous fourth-order fit of the ATZfc-14 400 data set (6D-1) with 76 parameters yielded a rms deviation of 5.3 cm^{-1}. Striving for analytical functions that are as compact as possible, we have tried to carefully minimize the number of varied parameters in each fit (171 out of 303 parameters in the preceding example).

The *ab initio* energy values and the parameter values obtained from the fits of the potential-energy function in Eq. (2) are given as supplementary material[38] for each of the data sets in Table I, together with FORTRAN routines for evaluating the corresponding potential-energy functions at any geometry. The CBS**-5 potential-energy surface is expected to provide the best overall description of the electronic ground state of NH_3 below 20 000 cm^{-1} (see Sec. VIII), and therefore we list the parameters for this surface in Tables II and III. Further information about the quality of the fits is given in Sec. VI.

V. VARIATIONAL CALCULATIONS

The quality of the constructed potential-energy surfaces can be assessed by variationally computing the vibrational term values of $^{14}NH_3$ and comparing the results with experiment. Our variational approach to the calculation of rotation-vibration energies[1,9] and intensities[7,8] of XY_3 pyramidal molecules is an implementation of the Hougen-Bunker-Johns (HBJ) formalism.[39] The molecular motion is described by

TABLE III. CBS**-5 quintic and sextic potential-energy parameters (see caption of Table II) (in cm^{-1}) for the electronic ground state of NH_3.

Parameter	Value	Parameter	Value	Parameter	Value
f^0_{44444}	−127.4(12)	f^0_{13345}	−679.2(80)	f^1_{24445}	−8 199(162)
f^1_{44444}	1 827(24)	f^0_{12355}	221(13)	f^2_{24445}	56 324(1357)
f^2_{44444}	9 830(378)	f^0_{11334}	624.3(69)	f^0_{23344}	1 130(27)
f^0_{33455}	−714(11)	f^1_{11334}	2 211(120)	f^0_{23344}	−440(15)
f^2_{33455}	−108 147(2062)	f^0_{11255}	807.3(72)	f^1_{23344}	−3 746(264)
f^0_{33445}	809.8(39)	f^2_{11255}	−27 721(1211)	f^2_{23334}	−144 810(5072)
f^1_{33445}	3 330(66)	f^1_{11245}	−3 018(196)	f^1_{22335}	11 246(422)
f^0_{33345}	1 791(14)	f^2_{11245}	43 059(2393)	f^0_{22233}	−578(29)
f^1_{33345}	4 219(260)	f^1_{11135}	−7 232(158)	f^0_{22225}	−1 648(20)
f^0_{33344}	−2 410.4(82)	f^0_{11134}	245.9(76)	f^0_{22224}	−2 032(38)
f^1_{33344}	−11 427(177)	f^0_{11123}	−400(15)	f^1_{22224}	−34 578(738)
f^2_{33344}	50 287(1419)	f^1_{55555}	2 257(43)	f^2_{22224}	211 698(4360)
f^0_{33334}	−183.1(45)	f^2_{55555}	24 161(483)	f^0_{22222}	−458(12)
f^0_{33333}	1 749.4(49)	f^0_{44444}	127.07(87)	f^1_{22222}	5 104(120)
f^0_{25555}	−52.8(23)	f^1_{44444}	4 563(47)	f^0_{14555}	−1 719(11)
f^1_{25555}	−1 133(30)	f^2_{44444}	42 425(542)	f^1_{14555}	−27 172(221)
f^2_{25555}	−17 384(598)	f^0_{33555}	121.1(71)	f^2_{14555}	82 494(1883)
f^0_{24455}	584.9(49)	f^2_{33555}	−19 542(463)	f^0_{13444}	−336.8(82)
f^2_{24455}	−53 324(1258)	f^0_{33445}	867(15)	f^1_{13444}	−4 362(90)
f^0_{24445}	1 070.1(53)	f^1_{33445}	4 471(227)	f^0_{13344}	661(17)
f^1_{24445}	4 655(76)	f^0_{33444}	−1 066(16)	f^1_{13333}	5 970(212)
f^2_{24445}	−37 568(1244)	f^1_{33444}	−6 945(258)	f^2_{13333}	−72 281(2700)
f^0_{23333}	−374.9(60)	f^0_{33355}	560(15)	f^0_{12455}	1 027(19)
f^0_{13455}	1 127(11)	f^1_{33355}	−4 979(120)	f^1_{12455}	10 494(230)
f^1_{13455}	7 287(161)	f^0_{33333}	619(18)	f^0_{12445}	254(16)
f^2_{13455}	27 647(2367)	f^1_{33333}	7 177(280)	f^0_{12345}	−733(62)
f^0_{13445}	−395(54)	f^0_{24455}	−648(12)	f^0_{11355}	−828(16)
f^1_{13445}	−2 037(87)	f^1_{24455}	−14 993(220)	f^1_{11355}	−2 148(162)
f^2_{13445}	21 076(1148)	f^0_{24445}	−493.8(87)	f^0_{11144}	−266(20)

means of a flexible *reference configuration* (of $\mathcal{C}_{3v}$ geometrical symmetry for NH_3) that follows the large-amplitude motions (rotation and inversion), whereas the remaining vibrations are viewed as small-amplitude displacements from the reference configuration. In our model, these small-amplitude displacements are measured by the linearized coordinates $r_k^{(\ell)}$, $k=1,2,3$, and

$$S^{\ell}_{4a} = \frac{1}{\sqrt{6}}(2\alpha^{\ell}_1 - \alpha^{\ell}_2 - \alpha^{\ell}_3), \tag{9}$$

$$S^{\ell}_{4b} = \frac{1}{\sqrt{2}}(\alpha^{\ell}_2 - \alpha^{\ell}_3). \tag{10}$$

Here, $r_k^{(\ell)}$ is the linearized version[9] of the bond length r_k, and α_k^{ℓ} is the linearized version of the bond angle α_k. The coordinates $r_k^{(\ell)}$, $k=1,2,3$, and $(S^{\ell}_{4a}, S^{\ell}_{4b})$ describe the stretching motion and the degenerate bending mode, respectively. The inversion is represented by the HBJ inversion coordinate[9] ρ which, in the reference configuration, is the angle between the $\mathcal{C}_3$ rotational symmetry axis and any one of the N–H bonds. The rotational motion is described by means of a molecule-fixed axis system xyz defined by the Eckart-Sayvetz conditions.[40,41] By implementing the Eckart-Sayvetz conditions, we obtain a Hamiltonian with the largest possible separation between different types of motion, in particular, between rotation and vibration, which facilitates calculations on highly excited rotational states.[42] A drawback of the Eckart-Sayvetz conditions, however, is that they lead to a nuclear kinetic-energy operator expressed as a truncated expansion (with ρ-dependent expansion coefficients) in the small-amplitude vibrational coordinates. In our model, these coordinates are

$$y^{\ell}_k = 1 - \exp[-a(r_k^{(\ell)} - r_e)], \quad k = 1,2,3, \tag{11}$$

S^{ℓ}_{4a}, and S^{ℓ}_{4b}. The kinetic-energy expansion was previously[1] truncated after the fourth order in y^{ℓ}_k and the first order in $(S^{\ell}_{4a}, S^{\ell}_{4b})$, but the code has later been extended such that this expansion can be taken through eighth order in all coordinates.[9] In the currently implemented model, the potential-energy function is transformed to a sixth-order expansion in all coordinates, while a fourth-order expansion was employed originally.[1]

In the variational nuclear-motion calculations, a truncated matrix representation of the rotation-vibration Hamiltonian is diagonalized. The basis set is constructed from Morse oscillator functions (labeled by the principal quantum numbers n_1, n_2, and n_3) for the local stretching modes, two-dimensional isotropic harmonic oscillator functions (labeled by the principal quantum number n_b) for the bending modes, and numerical inversion functions (labeled by the principal quantum number n_i) obtained by solving the one-dimensional inversion Schrödinger problem with the

TABLE IV. *Ab initio* potential-energy surfaces for the electronic ground state of NH_3.

		Fit[a]				Variational calculations for $^{14}NH_3$[b]		
	PES	N_{pts}	E_{max} (cm^{-1})	N_{prm}	σ_{rms} (cm^{-1})	$\delta_{10\,300}$ (cm^{-1})	δ_{6100} (cm^{-1})	δ_{split} (cm^{-1})
1	ATZfc-1	14 400	36 800	128	1.2	32.5	20.7	13.5
2	ATZfc-4	45 760	36 800	147	0.9	30.5	20.2	12.9
3	ATZfc-5	51 816	36 800	171	3.5	30.0	20.8	13.2
4	CBS+	3 814	36 000	163	7.2	8.8	5.8	1.2
5	CBS**-4	45 760	36 000	140	1.4	7.9	4.3	1.9
6	CBS**-5	51 816	36 000	181	3.6	9.4	6.3	1.3
7	ATZfc(2002)	14 400	36 800	76	5.3	32.6(35.0)[c]	22.4	13.5
8	CBS+(2002)	1 236	36 000	69	6.4	18.8(11.5)[c]	18.8	3.0

[a] N_{pts}, E_{max}, N_{prm}, and σ_{rms} are the number of *ab initio* points in the data set, the maximum *ab initio* energy in the data set relative to the equilibrium energy, the number of parameters varied, and the rms deviation obtained in the fitting of the *ab initio* points, respectively (see text).

[b] $\delta_{10\,300}$, δ_{6100}, and δ_{split} are the rms deviations between observed and calculated values for the vibrational term values below 10 300 cm^{-1}, the vibrational term values below 6100 cm^{-1}, and the inversion splittings for the vibrational states below 10 300 cm^{-1}, respectively.

[c] The quantity given in parentheses is the value of $\delta_{10\,300}$ obtained from variational calculations using the earlier implementation in Ref. 1 (see text).

Numerov-Cooley approach[43–45] on a numerical grid of $N_{inv}=1000$ points. The basis set used in the variational calculations is truncated according to

$$P = 2(n_1 + n_2 + n_3) + n_i + n_b \leq P_{max}. \quad (12)$$

Convergence tests show that at $P_{max}=18$, the convergence is better than 0.1 cm^{-1} for the energies listed in Table V. For $P_{max}=14$, we obtain convergence to within 0.6 cm^{-1}. We use the $P_{max}=14$ basis set in most standard calculations, and $P_{max}=18$ when higher accuracy is important. For $P_{max}=14$, the matrix blocks to be diagonalized for $J=0$ have the dimensions $N_A=1455$ [A symmetry in $\mathcal{D}_{3h}(M)$] and $N_E=2571$ (E symmetry), while for $P_{max}=18$, $N_A=4486$ and $N_E=8241$. Test calculations with the nuclear kinetic-energy operator expanded to sixth and eighth order in the small-amplitude vibrational coordinates show differences in the calculated energies of less than 0.02 cm^{-1}. Thus, the sixth-order expansion is adequate and is adopted both for the kinetic- and potential-energy operators in the present work. All calculations reported in this paper refer to the rotational ground state ($J=0$).

VI. POTENTIAL-ENERGY SURFACES

We now describe and compare the six potential-energy surfaces listed in Table I and the two surfaces ATZfc(2002) and CBS+(2002) obtained previously.[1,46] It should be noted that the surfaces ATZfc(2002) and ATZfc-1 were determined by fitting to the same 14 400 *ab initio* points (grid 6D-1). However, they are different since the expansion in Eq. (2) was truncated after the fourth and sixth order, respectively. Table IV lists some characteristic properties of these eight surfaces, namely, the number of *ab initio* points N_{pts} in the underlying grid, the highest *ab initio* energy E_{max} (relative to the equilibrium energy) in the data set, the number of parameters N_{prm} varied during the fitting, and the rms deviation σ_{rms} of the fit. For each of these surfaces, variational calculations of the vibrational term values were carried out for $^{14}NH_3$ as described in Sec. V, and the resulting rms deviations from experiment are included in Table IV for the energies below 10 300 cm^{-1}($\delta_{10\,300}$), the energies below 6100 cm^{-1}(δ_{6100}), and the inversion splittings below 10 300 cm^{-1}(δ_{split}).

We evaluate the constructed potential-energy surfaces with regard to the quality of the fits (Sec. VI A), the calculated vibrational term values (Sec. VI B), and the calculated vibrational transition moments (Sec. VI C).

A. Quality of the fits

Inspection of Table IV shows that the rms deviations of the analytical fits to the *ab initio* energies are reasonably low. They lie between 0.9 and 1.4 cm^{-1} for sixth-order expansions in the internal region (ATZfc-1, ATZfc-4, and CBS**-4), between 5.3 and 6.4 cm^{-1} for fourth-order expansions in the internal region [ATZfc(2002) and CBS+(2002)], and between 3.5 and 7.2 cm^{-1} for sixth-order expansions that cover all points including those in the border region (ATZfc-5, CBS+, and CBS**-5).

The transition from the previously used fourth-order expansions[1] to sixth-order expansions has improved the quality of the fits significantly. This is seen most clearly for the ATZfc-14 400 data set where the rms deviation has been reduced from 5.3 to 1.2 cm^{-1}, at the expense of having 128 rather than 76 optimized parameters. Therefore we generally recommend to truncate the analytical potential-energy function in Eq. (2) only after the sixth order.

The points in the border region with their distorted geometries are harder to fit than those in the internal region. In the case of the ATZfc-5 and CBS**-5 surfaces, only 12% of the *ab initio* points lie in the border region, and standard fits with unit weight for all points yield acceptable results (rms deviations of 3.5 and 3.6 cm^{-1} overall, and 1.7 and 1.8 cm^{-1} for the internal region). In the case of the CBS+ surface, however, 62% of the points lie in the border region, and we have therefore assigned weights of 10 to the internal points and 1 to the border points to make sure that the spectroscopically important internal region is well represented by the fit;

this has led to rms deviations of 7.2 cm^{-1} overall and 2.5 cm^{-1} for the internal region (compared with 6.5 and 4.2 cm^{-1} from a standard fit with unit weights).

The internal consistency between different fits can be checked most easily for the ATZfc-based surfaces. The rms deviation between the ATZfc-1 and ATZfc-5 potential functions, calculated at the 14 400 common geometries in 6D-1, is less than 2 cm^{-1}, and the same is true for the rms deviation between ATZfc-4 and ATZfc-5, calculated at the 45 760 common geometries in 6D-5. These three sixth-order expansions are thus quite similar in the internal region.

Extrapolations beyond the fitting domain are generally associated with larger errors. Taking the fourth-order ATZfc(2002) expansion as an example, the rms deviations with regard to the ATZfc-14400, ATZfc-45760, and ATZfc-51816 data sets are 5.3, 16.0, and 50.2 cm^{-1}, respectively. Obviously, the extrapolation is particularly difficult for the ATZfc-51816 set that contains the distorted geometries of the border region. This is confirmed by the rms deviations of the six-order ATZfc-1 and ATZfc-4 expansions for the ATZfc-51816 data set which amount to 90 and 96 cm^{-1}, respectively.

In summary, the *ab initio* energies in the spectroscopically important internal region near equilibrium can be represented analytically with an accuracy of about 1 cm^{-1}; in the case of the most accurate CBS**-4 surface the rms deviation is 1.4 cm^{-1} for 45 760 energies. Inclusion of the border points provides the desired complete coverage up to 20 000 cm^{-1} above equilibrium, but makes the analytic fits more difficult; for the most accurate CBS**-5 surface, the rms deviation rises to 3.6 cm^{-1} for 51 816 energies. Both the CBS**-4 and the CBS**-5 surface give an inversion barrier of 1792 cm^{-1}, close to the directly computed[1] CBS+ value of 1790 cm^{-1}.

B. Vibrational term values

Experimentally determined vibrational term values for $^{14}NH_3$ and the corresponding theoretical values calculated from the ATZfc-5, CBS+, and CBS**-5 potential-energy surfaces (see Tables I and IV) are listed in Table V. The vibrational states are labeled by the quantum numbers v_1, v_2^p, $v_3^{l_3}$, and $v_4^{l_4}$, where v_r and l_r are the usual harmonic oscillator quantum numbers, and $p=+(-)$ indicates the lower, symmetric (upper, antisymmetric) inversion component. The quantity Γ is the symmetry of the vibrational state in the molecular symmetry group[35,36] $\mathcal{D}_{3h}(M)$. Theoretical and experimental values for the $J=0$ inversion splittings of $^{14}NH_3$ are compared in Table VI; the theoretical values are determined from the ATZfc-5, CBS+, and CBS**-5 potential-energy surfaces, and the vibrational states are labeled as in Table V.

As shown in Sec. VI A, all ATZfc-based surfaces considered presently are rather similar in the spectroscopically important internal region (6D-4 grid). It is therefore not surprising that the calculated vibrational term values are of similar quality, with typical rms deviations from experiment (see Table IV) of $\delta_{10\,300}\approx 30$ cm^{-1}, $\delta_{6100}\approx 21$ cm^{-1}, and $\delta_{\text{split}}\approx 13$ cm^{-1}. The improvements in the nuclear-motion model (see Sec. V) lead to slightly better vibrational energies in the case of ATZfc(2002): $\delta_{10\,300}$ drops from 35.0 cm^{-1} previously[1] to 31.2 cm^{-1}.

The agreement between experimental and theoretical vibrational term values is improved substantially at higher levels of *ab initio* theory, i.e., when using the CBS+, CBS**-4, and CBS**-5 potential-energy surfaces. In all three cases, the rms deviations from experiment lie in a narrow range: $\delta_{10\,300}$ between 7.9 and 9.4 cm^{-1}, δ_{6100} between 4.3 and 6.3 cm^{-1}, and δ_{split} between 1.2 and 1.9 cm^{-1} (see Table IV). The CBS**-4 surface gives the best results for the vibrational term values, while it is slightly inferior to the other two surfaces for the inversion splittings, but the differences are only minor. Compared with the ATZfc-based surfaces, the rms deviations of the higher-level results are lowered by a factor of 4 for the vibrational term values, and by an order of magnitude for the inversion splittings. There are also improvements relative to the CBS+(2002) surface (see Table IV) where the use of the refined nuclear-motion model has increased $\delta_{10\,300}$ from 11.5 cm^{-1} previously[1] to 18.8 cm^{-1}.

C. Vibrational transition moments

Transition moments for selected vibrational transitions in the electronic ground state of $^{14}NH_3$ are listed in Table VII. They are defined as

$$\mu_{fi}=\sqrt{\sum_{\alpha=x,y,z}|\langle\Phi_{\text{vib}}^{(f)}|\bar{\mu}_\alpha|\Phi_{\text{vib}}^{(i)}\rangle|^2}, \tag{13}$$

where $\bar{\mu}_\alpha$ is a component of the electronically averaged molecular dipole moment along the molecule-fixed axis[9] $\alpha=x$, y, or z, while $\Phi_{\text{vib}}^{(i)}$ and $\Phi_{\text{vib}}^{(f)}$ are the vibrational wave functions of the initial state i and the final state f, respectively. In the calculation of μ_{fi}, we use the ATZfc dipole moment function.[1,7,8] The required matrix elements are generated by techniques described previously.[9] The vibrational wave functions $\Phi_{\text{vib}}^{(w)}$, $w=i$ or f, are calculated variationally on the ATZfc-5, CBS+, and CBS**-5 surfaces. We consider transitions originating in the vibrational ground-state inversion components 0^+ (the lower, symmetric component) and 0^- (the upper, antisymmetric component). If the final state f of the transition has the symmetry $\Gamma=A''$ or E' in $\mathcal{D}_{3h}(M)$, the initial state is 0^+; if the final state has A' or E'' symmetry, the initial state is 0^-. The upper states f are labeled as in Tables V and VI.

The three calculations use different vibrational wave functions, but the same ATZfc dipole moment surface. It is therefore not surprising that the three sets of computed transition moments are quite similar, with deviations typically in the percent range (see Table VII); moreover, all of them are in very satisfactory agreement with the available experimental results. The largest discrepancies between the computed transition moments are found for the transitions $2\nu_2^{\pm}\leftarrow 0^{\mp}$ where the ATZfc values amount to only 70% of the CBS+ and CBS**-5 values. A possible explanation is that the upper states of these two transitions are close to the top of the inversion barrier that is overestimated at the ATZfc level by

TABLE V. Vibrational term values (in cm^{-1}) for the electronic ground state of $^{14}NH_3$.

State							ATZfc-5		CBS+		CBS**-5	
Γ	v_1	v_2^p	$v_3^{l_3}$	$v_4^{l_4}$	Obs.	Ref.[a]	Calc.	O–C[b]	Calc.	O–C[b]	Calc.	O–C[b]
A'	0	1^+	0^0	0^0	932.43	51	961.25	−28.82	933.76	−1.33	934.25	−1.82
	0	2^+	0^0	0^0	1 597.47	52	1 666.12	−68.65	1 599.78	−2.31	1 601.31	−3.84
	0	3^+	0^0	0^0	2 384.15	53	2 408.09	−23.94	2 387.77	−3.62	2 388.55	−4.40
	0	0^+	0^0	2^0	3 216.10	54	3 211.07	5.03	3 220.62	−4.52	3 221.15	−5.05
	1	0^+	0^0	0^0	3 336.11	54	3 319.42	16.69	3 342.37	−6.26	3 342.24	−6.13
	0	4^+	0^0	0^0	3 462	55	3 455.11	6.89	3 467.91	−5.91	3 468.33	−6.33
	0	1^+	0^0	2^0	4 115.62	56	4 148.15	−32.53	4 121.45	−5.83	4 123.01	−7.39
	1	1^+	0^0	0^0	4 294.53	56	4 302.33	−7.80	4 302.27	−7.74	4 302.46	−7.93
	1	0^+	0^0	2^0	6 520	57	6 492.65	27.35	6 530.84	−10.84	6 531.38	−11.38
	2	0^+	0^0	0^0	6 606.0	57	6 623.60	−17.60	6 616.80	−10.80	6 617.45	−11.45
	0	0^+	2^0	0^0	6 795.30	57	6 750.30	45.00	6 808.88	−13.58	6 809.47	−14.17
	0	0^+	3^3	0^0	10 232.52	57	10 164.36	68.16	10 252.22	−19.70	10 253.36	−20.84
E'	0	0^+	0^0	1^1	1 626.28	52	1 624.89	1.39	1 628.57	−2.29	1 628.84	−2.56
	0	1^+	0^0	1^1	2 540.53	53	2 571.38	−30.85	2 543.80	−3.27	2 544.77	−4.24
	0	0^+	0^0	2^2	3 240.44	54	3 255.44	−15.00	3 244.84	−4.40	3 245.41	−4.97
	0	0^+	1^1	0^0	3 443.68	55	3 420.34	23.34	3 449.20	−5.52	3 449.35	−5.67
	0	1^+	0^0	2^2	4 135.94	56	4 169.11	−33.17	4 141.40	−5.46	4 143.00	−7.06
	0	1^+	1^1	0^0	4 416.91	56	4 416.90	0.01	4 423.65	−6.74	4 424.41	−7.50
	1	0^+	0^0	1^1	4 955.85	57	4 938.54	17.31	4 965.04	−9.19	4 965.03	−9.18
	0	0^+	1^1	1^1	5 052.60	57	5 027.76	24.84	5 060.69	−8.09	5 061.24	−8.64
	0	1^+	1^1	1^1	6 012.90	57	6 013.73	−0.83	6 021.43	−8.53	6 022.97	−10.07
	1	0^+	0^0	2^2	6 566.22	57	6 575.13	−8.91	6 568.43	−2.21	6 568.95	−2.73
	1	0^+	1^1	0^0	6 608.83	57	6 643.03	−34.20	6 618.61	−9.78	6 620.27	−11.44
	0	0^+	1^1	2^{-2}	6 677.23	57	6 647.40	29.83	6 677.60	−0.37	6 678.46	−1.23
	0	0^+	2^2	0^0	6 850.20	57	6 804.92	45.28	6 861.73	−11.53	6 862.03	−11.83
	2	0^+	0^0	1^1	8 200	58	8 173.85	26.15	8 220.50	−20.50	8 222.37	−22.37
	0	0^+	3^1	0^0	10 110.86	57	10 049.90	60.96	10 129.87	−19.01	10 131.20	−20.34
A''	0	0^-	0^0	0^0	0.79	51	0.49	0.30	0.79	0.00	0.79	0.00
	0	1^-	0^0	0^0	968.12	51	985.10	−16.98	969.51	−1.39	969.73	−1.61
	0	2^-	0^0	0^0	1 882.18	52	1 904.10	−21.92	1 884.96	−2.78	1 885.51	−3.33
	0	3^-	0^0	0^0	2 895.51	53	2 899.14	−3.63	2 900.01	−4.50	2 900.49	−4.98
	0	0^-	0^0	2^0	3 217.78	54	3 212.16	5.62	3 222.25	−4.47	3 222.77	−4.99
	1	0^-	0^0	0^0	3 337.10	54	3 320.19	16.91	3 343.34	−6.24	3 343.22	−6.12
	0	4^-	0^0	0^0	4 055[c]	59	4 042.85	12.15	4 068.25	−13.25	4 068.53	−13.53
	0	1^-	0^0	2^0	4 173.25	56	4 186.75	−13.50	4 179.06	−5.81	4 180.06	−6.81
	1	1^-	0^0	0^0	4 320.04	56	4 319.82	0.22	4 327.91	−7.87	4 327.94	−7.90
	0	0^-	2^0	0^0	6 796.73	57	6 751.13	45.60	6 807.22	−10.49	6 807.85	−11.12
	0	0^-	3^3	0^0	10 234.73	57	10 165.04	69.69	10 250.07	−15.34	10 250.62	−15.89
E''	0	0^-	0^0	1^1	1 627.37	52	1 625.57	1.80	1 629.68	−2.31	1 629.95	−2.58
	0	1^-	0^0	1^1	2 586.13	53	2 602.04	−15.91	2 589.62	−3.49	2 590.21	−4.08
	0	0^-	0^0	2^2	3 241.62	54	3 238.06	3.56	3 246.30	−4.68	3 246.88	−5.26
	0	0^-	1^1	0^0	3 443.99	55	3 420.55	23.44	3 449.57	−5.58	3 449.71	−5.72
	0	1^-	0^0	2^2	4 193.14	56	4 207.70	−14.56	4 198.89	−5.75	4 200.04	−6.90
	0	1^-	1^1	0^0	4 435.44	56	4 428.88	6.56	4 442.34	−6.90	4 442.93	−7.49
	1	0^-	0^0	1^1	4 956.79	57	4 939.37	17.42	4 966.18	−9.39	4 966.24	−9.45
	0	0^-	1^1	1^1	5 052.97	57	5 028.10	24.87	5 061.31	−8.34	5 061.91	−8.94
	0	1^-	1^1	1^1	6 037.12	57	6 028.85	8.27	6 045.42	−8.30	6 046.70	−9.58
	1	0^-	0^0	2^2	6 566.22	57	6 575.97	−9.75	6 569.92	−3.70	6 570.54	−4.32
	1	0^-	1^1	0^0	6 609.66	57	6 641.50	−31.84	6 619.55	−9.89	6 621.29	−11.63
	0	0^-	1^1	2^{-2}	6 677.95	57	6 647.76	30.19	6 677.35	0.60	6 678.48	−0.53
	0	0^-	2^2	0^0	6 850.70	57	6 805.09	45.61	6 862.14	−11.44	6 862.45	−11.75
	0	0^-	3^1	0^0	10 111.31	57	10 049.78	61.53	10 130.68	−19.37	10 131.76	−20.45
					δ_{6100}[d]			20.77		5.78		6.33
					$\delta_{10\,300}$[e]			29.97		8.77		9.44

[a]Reference for the experimentally derived (observed) vibrational term values.
[b]Residual (observed-calculated) in cm^{-1}.
[c]The $(0,4^-,0^0,0^0)$ term value is not included in calculations of rms deviations because of its high experimental uncertainty (see Ref. 59).
[d]rms deviation (in cm^{-1}) between observed and calculated vibrational term values below 6100 cm^{-1}.
[e]rms deviation (in cm^{-1}) between observed and calculated vibrational term values below 10 300 cm^{-1}.

TABLE VI. Observed and calculated inversion splittings for $^{14}NH_3$ (in cm^{-1}).

State					Obs.[a]			ATZfc-5		CBS+		CBS**-5	
Γ	v_1	v_2	$v_3^{l_3}$	$v_4^{l_4}$	E_+	E_-	Δ	Calc.[b]	O–C[c]	Calc.[b]	O–C[c]	Calc.[b]	O–C[c]
A	0	0	0^0	0^0	0.00	0.79	0.79	0.49	0.30	0.79	0.00	0.79	0.00
	0	1	0^0	0^0	932.43	968.12	35.69	23.85	11.84	35.75	−0.06	35.48	0.21
	0	2	0^0	0^0	1 597.47	1 882.18	284.71	237.98	46.73	285.18	−0.47	284.20	0.51
	0	3	0^0	0^0	2 384.15	2 895.51	511.36	491.05	20.31	512.24	−0.88	511.94	−0.58
	0	0	0^0	2^0	3 216.10	3 217.78	1.68	1.09	0.59	1.63	0.05	1.62	0.06
	1	0	0^0	0^0	3 336.11	3 337.10	0.99	0.77	0.22	0.97	0.02	0.98	0.01
	0	1	0^0	2^0	4 115.62	4 173.25	57.63	38.60	19.03	57.61	0.02	57.05	0.58
	1	1	0^0	0^0	4 294.53	4 320.04	25.51	17.49	8.02	25.64	−0.13	25.48	0.03
	0	0	2^0	0^0	6 795.30	6 796.73	1.43	0.83	0.60	−1.66	3.09	−1.62	3.05
	0	0	3^3	0^0	10 232.52	10 234.73	2.21	0.68	1.53	−2.15	4.36	−2.74	4.95
E	0	0	0^0	1^1	1 626.28	1 627.37	1.09	0.68	0.41	1.11	−0.02	1.11	−0.02
	0	1	0^0	1^1	2 540.53	2 586.13	45.60	30.66	14.94	45.82	−0.22	45.44	0.16
	0	0	0^0	2^2	3 240.44	3 241.62	1.18	−17.38	18.56	1.46	−0.28	1.47	−0.29
	0	0	1^1	0^0	3 443.68	3 443.99	0.31	0.21	0.10	0.37	−0.06	0.36	−0.05
	0	1	0^0	2^2	4 135.94	4 193.14	57.20	38.59	18.61	57.49	−0.29	57.04	0.16
	0	1	1^1	0^0	4 416.91	4 435.44	18.53	11.98	6.55	18.69	−0.16	18.52	0.01
	1	0	0^0	1^1	4 955.85	4 956.79	0.94	0.83	0.11	1.14	−0.20	1.21	−0.27
	0	0	1^1	1^1	5 052.60	5 052.97	0.37	0.34	0.03	0.62	−0.25	0.67	−0.30
	0	1	1^1	1^1	6 012.90	6 037.12	24.22	15.12	9.10	23.99	0.23	23.73	0.49
	1	0	0^0	2^2	6 566.22	6 566.22	0.00	0.84	−0.84	1.49	−1.49	1.59	−1.59
	1	0	1^1	0^0	6 608.83	6 609.66	0.83	−1.53	2.36	0.94	−0.11	1.02	−0.19
	0	0	1^1	2^{-2}	6 677.23	6 677.95	0.72	0.36	0.36	−0.25	0.97	0.02	0.70
	0	0	2^2	0^0	6 850.20	6 850.70	0.50	0.17	0.33	0.41	0.09	0.42	0.08
	0	0	3^1	0^0	10 110.86	10 111.31	0.45	−0.12	0.57	0.81	−0.36	0.56	−0.11
					δ_{split}[d]				13.2		1.2		1.3

[a] E_+ (E_-) is the term value of the lower, symmetric (upper, antisymmetric) inversion component and $\Delta = E_- - E_+$ is the inversion splitting. The references for the experimentally derived vibrational term values can be inferred from Table V.
[b] Calculated Δ value in cm^{-1}.
[c] Residual (observed-calculated) in cm^{-1}.
[d] rms deviation in cm^{-1}.

150 cm^{-1},[1,5] which may cause a drastic change in the $2\nu_2^{\pm}$ wave functions relative to those obtained at the CBS+ and CBS**-5 levels.

VII. REFINEMENT

Even with our best surfaces there are residual errors in the computed vibrational spectra relative to experiment. For further improvements on a purely *ab initio* basis, one would need to go beyond the current CCSD(T) level by including higher excitations in the coupled-cluster series, more accurate corrections for basis-set incompleteness, and additional terms such as diagonal Born-Oppenheimer corrections. Such improvements have been reported for NH_3,[6,25] and it has been established that these corrections can indeed cause changes of several wave numbers in the fundamental transitions of NH_3 and that wave-number accuracy can be reached in this manner.[6]

Here we explore a different strategy of surface refinement.[47] Following a commonly applied practice in spectroscopic work, we empirically adjust the *ab initio* surface by fitting to the experimental data that are available for the ground electronic state of NH_3. The number of optimized parameters is limited by truncating the potential-energy function in Eq. (2) after the fourth order. Accordingly the experimental input data comprise only the band centers below 6100 cm^{-1} (see Table V), except for the transition at 4055 cm^{-1} that has a large experimental uncertainty. To make sure that the refined surface remains close to the *ab initio* surface, the energies from the CBS**-45 760 set are included as input data. Separate weight factors are assigned to the experimental (W_i^{exp}) and the *ab initio* (W_i^{ref}) input data. In the refinement (see Ref. 47 for details), r_e and α_e are kept fixed at their CBS+ values, and hence 108 parameters are varied in the fitting to 34 term values and 45 760 CBS** energies. The parameter $R = W_i^{exp}/W_i^{ref}$ controls the relative importance of the two types of input data. For $R=0$ the potential parameters are fitted only to the *ab initio* energies and this leads to the results given in Sec. IV. On the other hand, for $1/R \to 0$ the refinement is unrestrained, and the surface is adjusted only to the experimental data.

Fits were done with several values of R gradually increasing from a starting value of $R=0$. For $R=0.001$ close agreement with experiment was achieved, with $\delta_{10\,300} \approx 3.0$ cm^{-1}, $\delta_{6100} \approx 0.4$ cm^{-1}, and $\delta_{split} \approx 0.8$ cm^{-1}. The resulting "spectroscopic" surface shows an rms deviation of 0.4 cm^{-1} from the experimental input data and of 8.9 cm^{-1} from the CBS** reference energies, and the inversion barrier is 1786.1 cm^{-1}, in excellent agreement with the best available[6] theoretical value of 1786.8 cm^{-1}. The refined potential parameters are given as supplementary material,[38] and

TABLE VII. Band centers ν_{fi} (in cm^{-1}) and vibrational transition moments μ_{fi} (in D) for $^{14}NH_3$ transitions originating in the vibrational ground state.

Final state f					ν_{fi}	μ_{fi}				
Γ	v_1	v_2^p	$v_3^{l_3}$	$v_4^{l_4}$	Obs.[a]	Obs.[b]	Ref.[c]	ATZfc-5	CBS+	CBS**-5
A'	0	1^+	0^0	0^0	932.43	0.248(7)	60	0.235 21	0.244 71	0.244 53
	0	2^+	0^0	0^0	1 597.47	0.020 36(25)	52	0.013 87	0.020 42	0.020 19
	0	3^+	0^0	0^0	2 384.15	0.004 96(13)	53	0.005 51	0.005 39	0.005 40
	0	0^+	0^0	2^0	3 216.10	0.009 20(6)	55	0.009 25	0.007 39	0.007 26
	1	0^+	0^0	0^0	3 336.11	0.026 2(1)	55	0.027 68	0.026 86	0.026 92
	0	4^+	0^0	0^0	3 462			0.001 99	0.002 01	0.002 03
	0	1^+	0^0	2^0	4 115.62			0.003 72	0.003 40	0.003 38
	1	1^+	0^0	0^0	4 294.51	0.007 9	61	0.008 39	0.008 72	0.008 73
	1	0^+	0^0	2^0	6 520			0.000 27	0.000 30	0.000 30
	2	0^+	0^0	0^0	6 606.0			0.000 20	0.000 10	0.000 08
	0	0^+	2^0	0^0	6 795.30			0.002 53	0.001 99	0.002 02
	0	0^+	3^3	0^0	10 232.52			0.000 29	0.000 24	0.000 30
E'	0	0^+	0^0	1^1	1 626.28	0.084 08(34)	52	0.081 50	0.082 83	0.082 79
	0	1^+	0^0	1^1	2 540.53	0.002 358(36)	53	0.009 30	0.009 03	0.009 08
	0	0^+	0^0	2^2	3 240.44	0.009 20(6)	55	0.008 51	0.009 12	0.009 08
	0	0^+	1^1	0^0	3 443.68	0.018 2(1)	55	0.015 09	0.018 10	0.018 10
	0	1^+	0^0	2^2	4 135.94			0.004 34	0.004 03	0.004 01
	0	1^+	1^1	0^0	4 416.91	0.020 6	61	0.024 28	0.024 60	0.024 60
	1	0^+	0^0	1^1	4 955.85			0.004 90	0.004 94	0.004 92
	0	0^+	1^1	1^1	5 052.60			0.015 46	0.015 82	0.015 80
	0	1^+	1^1	1^1	6 012.90			0.003 96	0.003 96	0.003 95
	1	0^+	0^0	2^2	6 566.22			0.004 32	0.003 28	0.003 11
	1	0^+	1^1	0^0	6 608.83			0.009 08	0.008 82	0.008 78
	0	0^+	1^1	2^{-2}	6 677.23			0.003 06	0.001 77	0.001 81
	0	0^+	2^2	0^0	6 850.20			0.002 73	0.002 86	0.002 88
	2	0^+	0^0	1^1	8 200			0.000 59	0.000 60	0.000 62
	0	0^+	3^1	0^0	10 110.86			0.000 87	0.000 92	0.000 93
A''	0	0^-	0^0	0^0	0.79	1.471 93(1)	62	1.475 00	1.456 20	1.456 37
	0	1^-	0^0	0^0	968.12	0.236(4)	60	0.228 72	0.234 79	0.234 70
	0	2^-	0^0	0^0	1 882.18	0.003 256(35)	52	0.001 27	0.002 72	0.002 65
	0	3^-	0^0	0^0	2 895.51	0.002 856(40)	53	0.002 62	0.002 70	0.002 70
	0	0^-	0^0	2^0	3 217.78	0.009 20(6)	55	0.009 33	0.007 51	0.007 37
	1	0^-	0^0	0^0	3 337.10	0.026 2(1)	55	0.027 78	0.026 96	0.027 02
	0	4^-	0^0	0^0	4 055			0.000 84	0.000 89	0.000 89
	0	1^-	0^0	2^0	4 173.25			0.004 03	0.003 78	0.003 76
	1	1^-	0^0	0^0	4 320.04	0.007 9	61	0.008 07	0.008 33	0.008 34
	0	0^-	2^0	0^0	6 796.73			0.002 53	0.002 52	0.002 51
	0	0^-	3^3	0^0	10 234.73			0.000 30	0.000 30	0.000 30
E''	0	0^-	0^0	1^1	1 627.37	0.084 08(34)	52	0.081 44	0.082 72	0.082 69
	0	1^-	0^0	1^1	2 586.13	0.002 182(82)	53	0.009 51	0.009 37	0.009 40
	0	0^-	0^0	2^2	3 241.62	0.009 20(6)	55	0.008 67	0.009 01	0.008 96
	0	0^-	1^1	0^0	3 443.99	0.018 2(1)	55	0.015 05	0.018 02	0.018 02
	0	1^-	0^0	2^2	4 193.14			0.004 76	0.004 55	0.004 52
	0	1^-	1^1	0^0	4 435.44	0.020 6	61	0.024 13	0.024 40	0.024 41
	1	0^-	0^0	1^1	4 956.79			0.004 89	0.004 91	0.004 88
	0	0^-	1^1	1^1	5 052.97			0.015 42	0.015 74	0.015 72
	0	1^-	1^1	1^1	6 037.12			0.004 01	0.003 99	0.003 98
	1	0^-	0^0	2^2	6 566.22			0.004 32	0.003 33	0.003 15
	1	0^-	1^1	0^0	6 609.66			0.009 04	0.008 82	0.008 78
	0	0^-	1^1	2^{-2}	6 677.95			0.002 76	0.001 79	0.001 84
	0	0^-	2^2	0^0	6 850.70			0.002 73	0.002 85	0.002 85
	0	0^-	3^1	0^0	10 111.31			0.000 89	0.000 90	0.000 92

[a]The references for the observed values of ν_{fi} can be inferred from Table V.
[b]Observed value of the vibrational transition moment with experimental uncertainty in parentheses (in units of the last digit quoted) where available.
[c]Reference for the experimental (observed) value of the vibrational transition moment.

the corresponding vibrational term values are listed in Table VIII. It is obvious that the low vibrational energies that were included in the fitting are well reproduced, typically within 1 cm^{-1} while there are errors of several wave numbers for the transitions above 6100 cm^{-1}, for example, in the case of the combination band $\nu_1+2\nu_4$.

TABLE VIII. Vibrational term values (in cm^{-1}) for the electronic ground state of $^{14}NH_3$. The calculated term values (Calc.) were obtained using a refined surface (see text for details). (See footnotes b and c of Table V.)

State						Refined		State						Refined	
Γ	v_1	v_2	$v_3^{l_3}$	$v_4^{l_4}$	Obs.	Calc.	O–C	Γ	v_1	v_2	$v_3^{l_3}$	$v_4^{l_4}$	Calc.	O–C	
A'	0	1^+	0^0	0^0	932.43	932.50	−0.07	A''	0	0^-	0^0	0^0	0.79	0.79	0.00
	0	2^+	0^0	0^0	1 597.47	1 597.46	0.01		0	1^-	0^0	0^0	968.12	968.16	−0.04
	0	3^+	0^0	0^0	2 384.15	2 384.15	0.00		0	2^-	0^0	0^0	1 882.18	1 882.13	0.05
	0	0^+	0^0	2^0	3 216.10	3 215.98	0.12		0	3^-	0^0	0^0	2 895.51	2 895.57	−0.06
	1	0^+	0^0	0^0	3 336.11	3 336.09	0.02		0	0^-	0^0	2^0	3 217.78	3 217.64	0.14
	0	4^+	0^0	0^0	3 462	3 462.80	−0.80		1	0^-	0^0	0^0	3 337.10	3 337.14	−0.04
	0	1^+	0^0	2^0	4 115.62	4 115.62	0.00		0	4^-	0^0	0^0	4 055	4 062.20	−7.20
	1	1^+	0^0	0^0	4 294.53	4 294.43	0.10		0	1^-	0^0	2^0	4 173.25	4 173.27	−0.02
	1	0^+	2^0	0^0	6 520	6 517.67	2.33		1	1^-	0^0	0^0	4 320.04	4 320.08	−0.04
	2	0^+	0^0	0^0	6 606.0	6 603.31	2.69		0	0^-	2^0	0^0	6 796.73	6 793.10	3.63
	0	0^+	2^0	0^0	6 795.30	6 795.29	0.01		0	0^-	3^3	0^0	10 234.73	10 232.40	2.33
	0	0^+	3^3	0^0	10 232.52	10 229.18	3.34								
E'	0	0^+	0^0	1^1	1 626.28	1 626.30	−0.02	E''	0	0^-	0^0	1^1	1 627.37	1 627.40	−0.03
	0	1^+	0^0	1^1	2 540.53	2 540.50	0.03		0	1^-	0^0	1^1	2 586.13	2 586.10	0.03
	0	0^+	0^0	2^2	3 240.44	3 240.15	0.29		0	0^-	0^0	2^2	3 241.62	3 241.63	−0.01
	0	0^+	1^1	0^0	3 443.68	3 443.72	−0.04		0	0^-	1^1	0^0	3 443.99	3 444.06	−0.07
	0	1^+	0^0	2^2	4 135.94	4 135.96	−0.02		0	1^-	0^0	2^2	4 193.14	4 193.17	−0.03
	0	1^+	1^1	0^0	4 416.91	4 416.89	0.02		0	1^-	1^1	0^0	4 435.44	4 435.48	−0.04
	1	0^+	0^0	1^1	4 955.85	4 955.70	0.15		1	0^-	0^0	1^1	4 956.79	4 956.94	−0.15
	0	0^+	1^1	1^1	5 052.60	5 052.71	−0.11		0	0^-	1^1	1^1	5 052.97	5 053.29	−0.32
	0	1^+	1^1	1^1	6 012.90	6 011.31	1.59		0	1^-	1^1	1^1	6 037.12	6 035.33	1.79
	1	0^+	0^0	2^2	6 566.22	6 554.92	11.30		1	0^-	0^0	2^2	6 566.22	6 556.47	9.75
	1	0^+	1^1	0^0	6 608.83	6 605.76	3.07		1	0^-	1^1	0^0	6 609.66	6 606.82	2.84
	0	0^+	1^1	2^{-2}	6 677.23	6 672.99	4.24		0	0^-	1^1	2^{-2}	6 677.95	6 673.78	4.17
	0	0^+	2^2	0^0	6 850.20	6 849.89	0.31		0	0^-	2^2	0^0	6 850.70	6 850.27	0.43
	2	0^+	0^0	1^1	8 200	8 208.76	−8.76		0	0^-	3^1	0^0	10 111.31	10 105.21	6.10
	0	0^+	3^1	0^0	10 110.86	10 104.89	5.97								

VIII. DISCUSSION AND CONCLUSION

The main goal of the present work was to construct a potential-energy surface for the electronic ground state of NH_3 that accurately covers the region up to 20 000 cm^{-1} above equilibrium. For this purpose, CCSD(T)-based energies were computed for 51 816 (3814) geometries at the ATZfc (CBS+) level, and these data were combined to generate at all 51 816 geometries CBS** energies which are expected to be essentially of CBS+ quality. The corresponding analytical representation (CBS**-5) is our best overall potential-energy function. Variational calculations on the CBS**-5 surface yield rms deviations of 1.3 and 6.3 cm^{-1} for the inversion splittings and the vibrational term values below 6100 cm^{-1}, respectively, relative to experiment. For these calculations, the distorted geometries in the border region of the CBS**-5 surface are less relevant, and therefore the CBS**-4 surface, which only covers the internal region close to equilibrium, may be slightly superior in spectroscopic applications, as indicated by an rms deviation of 4.3 cm^{-1} for the vibrational term values below 6100 cm^{-1}. Both these CCSD(T)-based surfaces fall short of the target accuracy of 1 cm^{-1} that has been advocated in recent work.[6,48,49] In the following, we therefore address the limitations of our approach and possible improvements.

One obvious shortcoming is the neglect of higher excitations in the coupled cluster series beyond CCSD(T). It has been shown recently[6,25] that their inclusion up to quintuple excitations (CCSDTQP) combined with an extrapolation to the full configuration-interaction (FCI) limit affects the computed vibrational term values of NH_3 significantly, for example, in the case of the symmetric and degenerate stretching fundamentals by −5.2 and −4.2 cm^{-1}, respectively.[6] Inspection of Table V shows that our variational calculations on the CBS**-5 surface consistently overestimate the experimental term values: in particular, all 12 transitions involving two or three quanta of the stretching modes have large absolute errors of 11–22 cm^{-1} which would be much reduced by assuming a transferable correction of about −5 cm^{-1} per stretching quantum (as indicated by CCSDTQP and FCI data; see above). There is a good chance, of course, that systematic corrections of this kind can be incorporated by an empirical surface refinement (see Sec. VII).

Another limitation of our current approach is the procedure for CBS extrapolation which employs the aug-cc-pVXZ basis sets with cardinal numbers $X=T,Q,5$. It has recently been argued in the case of water[48] that larger basis sets up to $X=7$ must be included in order to achieve an accuracy better than 1 cm^{-1}. Alternatively one may resort to the explicitly correlated R12 method to reach the CBS limit at the CCSD(T) level which caused changes up to 4 cm^{-1} in the computed fundamental wave numbers of NH_3 relative to CBS extrapolation.[6]

In our CBS+ calculations, the core-valence correlation energy is obtained as the difference between all-electron and frozen-core CCSD(T)/aug-cc-pCVTZ energies, which recovers only about 86% of the corresponding CCSD(T)/aug-cc-pCV5Z result.[1] This percentage is essentially constant over the spectroscopically relevant region so that the CBS+ energies could easily be corrected for this systematic error. This gives rise to changes of the order of 1 cm^{-1} in the calculated vibrational term values. Considering that other errors are larger (see above) we decided against including such a correction in the CBS+ scheme.

The relativistic corrections in CBS+ are evaluated at the CCSD(T)/aug-cc-pVTZ level as the sum of the expectation values for the mass-velocity and the one-electron Darwin terms. This should be adequate for a light molecule such as NH_3 even though more refined relativistic methods could be applied [which is mandatory for heavier molecules such as BiH_3 (Ref. 50)]. Diagonal Born-Oppenheimer corrections are not included in our approach. In NH_3 they affect the fundamental wave number for the inversion mode by 2.6 cm^{-1} and those for the other modes by less than 0.5 cm^{-1}.[6] It seems advisable to incorporate such corrections after taking care of other larger errors (see above).

When generating a potential-energy surface by *ab initio* calculations on a grid, the density of the points is considered to be an important factor for the accuracy that can be achieved.[48] Our largest grid (6D-5) contains 51 816 unique points (and many more symmetrically equivalent points), but being six dimensional it is still rather sparse. Moreover, the CBS^{**} construction scheme strongly depends on the number of points taken from the "parent" CBS+ data for the EDS fit (currently 3814 points): the denser the parent grid, the closer the CBS^{**} surface to the CBS+ limit, and the smaller the extrapolation error (which is presently 2.8 cm^{-1}). The analytical representation of the CBS^{**} energies necessarily introduces some further inaccuracies which can be assessed from the corresponding rms deviations (1.4 cm^{-1} for CBS^{**}-4 and 3.6 cm^{-1} for CBS^{**}-5).

Given the many caveats concerning accuracy, the pragmatic strategy of slightly adjusting a high-level *ab initio* surface to reproduce spectroscopic data seems attractive also in the case of NH_3. The refined surface obtained from a restrained fit to experimental and theoretical data indeed allows us to reproduce the observed vibrational term values below 6100 cm^{-1} almost exactly and leads to tolerable errors for the higher transitions up to 10 300 cm^{-1}. The chosen refinement is not unique, of course, but it provides a surface which can be an alternative, in spectroscopic work, to the purely *ab initio* surfaces developed presently.

The CBS^{**}-5 surface has the advantage that it affords a complete coverage of the energy range up to 20 000 cm^{-1} above equilibrium. While not perfect, it is highly accurate and available in analytical form. It should thus be useful in many applications, and it may serve as a component in global analytical potential-energy surfaces that extend into the dissociative regions.[10,11]

ACKNOWLEDGMENTS

This work was supported by the European Commission through Contract No. HPRN-CT-2000-00022, "Spectroscopy of Highly Excited Rovibrational States," and Contract No. MRTN-CT-2004-512202, "Quantitative Spectroscopy for Atmospheric and Astrophysical Research." The work of one of the authors (P.J.) is supported in part by the Deutsche Forschungsgemeinschaft and the Fonds der chemischen Industrie.

[1] H. Lin, W. Thiel, S. N. Yurchenko, M. Carvajal, and P. Jensen, J. Chem. Phys. **117**, 11265 (2002).
[2] C. Léonard, N. C. Handy, S. Carter, and J. M. Bowman, Spectrochim. Acta, Part A **58**, 825 (2002).
[3] C. Léonard, S. Carter, and N. C. Handy, Chem. Phys. Lett. **370**, 360 (2003).
[4] T. Rajamäki, A. Miani, and L. Halonen, J. Chem. Phys. **118**, 6358 (2003).
[5] T. Rajamäki, A. Miani, and L. Halonen, J. Chem. Phys. **118**, 10929 (2003).
[6] T. Rajamäki, M. Kálay, J. Noga, P. Valiron, and L. Halonen, Mol. Phys. **102**, 2297 (2004).
[7] S. N. Yurchenko, M. Carvajal, W. Thiel, H. Lin, and P. Jensen, Adv. Quantum Chem. **48**, 209 (2005).
[8] S. N. Yurchenko, M. Carvajal, H. Lin, J. J. Zheng, W. Thiel, and P. Jensen, J. Chem. Phys. **122**, 104317 (2005).
[9] S. N. Yurchenko, M. Carvajal, P. Jensen, H. Lin, J. J. Zheng, and W. Thiel, Mol. Phys. **103**, 359 (2005).
[10] F. Cuvelier, S. Hervé, R. Marquardt, and K. Sagui, Chimia **58**, 296 (2004).
[11] R. Marquardt, K. Sagui, W. Klopper, and M. Quack, J. Phys. Chem. B **109**, 8439 (2005).
[12] S. M. Colwell, S. Carter, and N. C. Handy, Mol. Phys. **101**, 523 (2003).
[13] E. Kauppi and L. Halonen, J. Chem. Phys. **103**, 6861 (1995).
[14] F. Gatti, J. Chem. Phys. **111**, 7225 (1999).
[15] F. Gatti, C. Iung, C. Leforestier, and X. Chapuisat, J. Chem. Phys. **111**, 7236 (1999).
[16] N. C. Handy, S. Carter, and S. M. Colwell, Mol. Phys. **96**, 477 (1999).
[17] D. Luckhaus, J. Chem. Phys. **113**, 1329 (2000).
[18] J. Pesonen, A. Miani, and L. Halonen, J. Chem. Phys. **115**, 1243 (2001).
[19] T. Rajamäki, A. Miani, J. Pesonen, and L. Halonen, Chem. Phys. Lett. **36**, 226 (2002).
[20] C. Léonard, S. Carter, and N. C. Handy, Chem. Phys. Lett. **370**, 360 (2003).
[21] H.-G. Yu and J. T. Muckerman, J. Mol. Spectrosc. **214**, 11 (2002).
[22] P. Rosmus, P. Botschwina, H.-J. Werner, V. Vaida, P. C. Engelking, and M. I. McCarthy, J. Chem. Phys. **86**, 6677 (1987).
[23] P. Pracna, V. Špirko, and W. P. Kraemer, J. Mol. Spectrosc. **136**, 317 (1989).
[24] R. Marquardt, M. Quack, I. Thanopulos, and D. Luckhaus, J. Chem. Phys. **119**, 10724 (2003).
[25] M. Kállay and J. Gauss, J. Chem. Phys. **120**, 6841 (2004).
[26] G. D. Purvis and R. J. Bartlett, J. Chem. Phys. **76**, 1910 (1982).
[27] M. Urban, J. Noga, S. J. Cole, and R. J. Bartlett, J. Chem. Phys. **83**, 4041 (1985).
[28] K. Raghavachari, G. W. Trucks, J. A. Pople, and M. Head-Gordon, Chem. Phys. Lett. **157**, 479 (1989).
[29] H.-J. Werner, P. J. Knowles, R. Lindh, M. Schýtz, and others, MOLPRO, version 2002.3, a package of *ab initio* programs (Birmingham, 2003).
[30] C. Hampel, K. Peterson, and H.-J. Werner, Chem. Phys. Lett. **190**, 1 (1992), and references therein; the program to compute the perturbative triples corrections has been developed by M. J. O. Deegan and P. J. Knowles, *ibid.* **227**, 321 (1994).
[31] T. H. Dunning, J. Chem. Phys. **90**, 1007 (1989).
[32] D. E. Woon and T. H. Dunning, J. Chem. Phys. **98**, 1358 (1993).
[33] D. Feller, J. Chem. Phys. **96**, 6104 (1992).
[34] D. Feller, J. Chem. Phys. **98**, 7059 (1993).
[35] P. R. Bunker and P. Jensen, *Molecular Symmetry and Spectroscopy*, 2nd ed. (NRC Research, Ottawa, 1998).
[36] P. R. Bunker and P. Jensen, *Fundamentals of Molecular Symmetry* (IOP, Bristol, 2004).

[37] T. J. Lee and P. R. Taylor, Int. J. Quantum Chem. Symp. **23**, 199 (1989).
[38] See EPAPS Document No. E-JCPSA6-123-004536. This document can be reached via a direct link in the online article's HTML reference section or via the EPAPS homepage (http://www.aip.org/pubservs/epaps.html).
[39] J. T. Hougen, P. R. Bunker, and J. W. C. Johns, J. Mol. Spectrosc. **34**, 136 (1970).
[40] C. Eckart, Phys. Rev. **47**, 552 (1935).
[41] A. Sayvetz, J. Chem. Phys. **7**, 383 (1939).
[42] S. N. Yurchenko, W. Thiel, S. Patchkovskii, and P. Jensen, Phys. Chem. Chem. Phys. **7**, 573 (2005).
[43] D. Papoušek, J. M. R. Stone, and V. Špirko, J. Mol. Spectrosc. **48**, 17 (1973).
[44] P. Jensen, Comput. Phys. Rep. **1**, 1 (1983).
[45] J. W. Cooley, Math. Comput. **15**, 363 (1961).
[46] We use the label (2002) to distinguish the potential-energy surfaces of Ref. 1 from those of the present work (Table I).
[47] S. N. Yurchenko, M. Carvajal, P. Jensen, F. Herregodts, and T. R. Huet, Chem. Phys. **290**, 59 (2003).
[48] O. L. Polyansky, A. G. Császár, S. V. Shirin, N. F. Zobov, P. Barletta, J. Tennyson, D. W. Schwenke, and P. J. Knowles, Science **299**, 539 (2003).
[49] A. D. Boese, M. Oren, O. Atasoylu, J. M. L. Martin, M. Kállay, and J. Gauss, J. Chem. Phys. **120**, 4129 (2004).
[50] J. Breidung, W. Thiel, D. Figgen, and H. Stoll, J. Chem. Phys. **120**, 10404 (2004).
[51] Š. Urban, V. Špirko, D. Papoušek, J. Kauppinen, S. P. Belov, L. I. Gershtein, and A. F. Krupnov, J. Mol. Spectrosc. **88**, 274 (1981).
[52] C. Cottaz, I. Kleiner, G. Tarrago, L. R. Brown, J. S. Margolis, R. L. Poynter, H. M. Pickett, T. Fouchet, P. Drossart, and E. Lellouch, J. Mol. Spectrosc. **203**, 285 (2000).
[53] I. Kleiner, G. Tarrago, and L. R. Brown, J. Mol. Spectrosc. **173**, 120 (1995).
[54] G. Guelachvili, A. H. Abdullah, N. Tu, K. N. Rao, and Š. Urban, J. Mol. Spectrosc. **133**, 345 (1989).
[55] I. Kleiner, L. R. Brown, G. Tarrago, Q.-L. Kou, N. Picqué, G. Guelachvili, V. Dana, and J.-Y. Mandin, J. Mol. Spectrosc. **193**, 46 (1999).
[56] Š. Urban, N. Tu, K. N. Rao, and G. Guelachvili, J. Mol. Spectrosc. **133**, 312 (1989).
[57] S. L. Coy and K. K. Lehmann, Spectrochim. Acta, Part A **45**, 47 (1989).
[58] H. Sasada, Opt. Lett. **9**, 448 (1984).
[59] L. D. Ziegler and B. Hudson, J. Phys. Chem. **88**, 1110 (1984).
[60] T. Nakanaga, S. Kondo, and S. Saëki, J. Mol. Spectrosc. **112**, 39 (1985).
[61] J. S. Margolis and Y. Y. Kwan, J. Mol. Spectrosc. **50**, 266 (1974).
[62] K. Tanaka, H. Ito, and T. Tanaka, J. Chem. Phys. **87**, 1557 (1987).